# *Combined Cr and S poisoning of $La_{0.8}Sr_{0.2}MnO_{3-\delta}$ (LSM) cathode of solid oxide fuel cells*

Cheng Cheng Wang[a,b,*], Shadi Darvish[c], Kongfa Chen[d], Bingxue Hou[e], Qi Zhang[e], Zanxiong Tan[a], Yu Zhong[c,*], San Ping Jiang[b,*]

[a]*Shen Zhen Polytechnic, Shenzhen, 518055, China*

[b]*Fuels and Energy Technology Institute & Department of Chemical Engineering, Curtin University, Perth, WA 6102, Australia*

[c]*Mechanical Engineering Department, Worcester Polytechnic Institute, Worcester, Massachusetts 01609, USA*

[d]*College of Materials Science and Engineering, Fuzhou University, Fujian 350108, PR China*

[e] *Panzhihua University, Panzhihua, 617000, China*

*Corresponding author:

sabrinachch_123@hotmail.com (Dr.C.C. Wang)

s.jiang@curtin.edu.au (Prof. Jiang SP)

## Abstract

Combined chromium and sulfur poisoning for $La_{0.8}Sr_{0.2}MnO_{3-\delta}$ (LSM) cathodes of solid oxide fuel cells (SOFCs) were investigated with cathodic current of 200 mA $cm^{-2}$ under 800 $^{o}$C for 22 hours. After polarization in chromium and sulfur at 800 $^{o}$C for 22 hours, polarization and ohmic resistance for LSM electrodes were 5.1 $\Omega \cdot cm^2$ and 7.62 $\Omega \cdot cm^2$, which were larger than values of LSM electrodes after chromium deposition only and sulfur deposition only. EDS, XPS and XRD results showed chromium and sulfur deposition occurred especially in bulk of the electrode, forming $SrCrO_4$ and $SrSO_4$. Compared with chromium deposition only, sulfur deposition only, combined chromium and sulfur deposition was not random and the degradation phenomenon of chromium and sulfur poisoning was much more severe. The combined chromium and sulfur deposition of LSM electrodes was induced by interaction among CrO, $SO_2$ and segregated SrO from LSM electrode. Thermodynamic predictions have been carried out utilizing CALPHAD approach, which were found in agreement with observed experimental results.



***Keywords:*** Solid oxide fuel cells; LSM electrodes; Chromium and sulfur deposition.


## 1. Introduction

Scientists are focusing on developing efficient methods to produce power. Solid oxide fuel cells (SOFCs) are excellent devices due to high energy conversion efficiency operating between 600 and 800 $^{o}$C [1-5]. For SOFCs to be commercial, they must exhibit durability as high as those of other conversion and storage devices. $La_{0.8}Sr_{0.2}MnO_{3-\delta}$ (LSM) [6] electrodes are used as cathodes for the oxygen reduction reaction (ORR) due to good electronic and catalytic activities, compatible with traditional YSZ. Moreover, LSM electrodes are always

operating at temperatures as high as 800 °C. However, one of technical problems is due to the performance deterioration relating to cathodes deactivation caused by contaminants including chromium (Cr), sulfur(S) and boron that can be in air or from glass sealant and so on [7-20]. Recently, NEDO projects regarding to the durability for SOFC stacks [21] have already showed interesting features related to degradation phenomenon. Major impurities influencing electrode performance can be regarded as chromium and sulfur for cathodes and phosphorus and sulfur for anodes.

Under operating temperature, Cr species were produced through chromium level, poisoned cathodes including LSM and LSCF and leaded to cell performance rapid degradation. Previous results have already shown that volatile Cr species deposited on electrode surface and/or interface, degrading the LSM cathodes performance [9, 22-24]. Chemical deposition was essentially a chemical reaction, induced by nucleation agents. Recently, Takeshi Daio et al. [25] reported that sulfur poisoning degradation phenomena of LSM cathodes by atomic-resolution analysis, who showed that $SrSO_4$ nano-particle and $La_2O_3$ was formed after exposed to $SO_2$. Our previous results indicated that sulfur deposition and poisoning was correlated with operating temperature and it was most severe at low temperature. Sulfur deposition at LSM electrode was initiated by chemical reaction among $SO_2$ and segregated SrO [15]. Deposition as well as poisoning of chromium and sulfur contaminants were previously studied on dense LSCF samples between 900 and 600 $^oC$ [26]. $SrCrO_4$ formed at 900 $^oC$ and 800 $^oC$, while $SrSO_4$ formed from 900 $^oC$ to 600 $^oC$.

The combining effect of Cr and S degradation on electrocatalytic performance for LSM and its potential mechanism has not been investigated extensively. In this paper, the

combining Cr and S poisoning and deposition on the electrocatalytic performance of LSM electrodes were investigated at 800 °C. All experimental results show that the interaction among Cr, S and LSM leaded to LSM decomposition, forming $SrCrO_4$ and $SrSO_4$ on the interface of LSM/YSZ, inner as well as outer surface of LSM electrodes. The deposition at LSM electrodes was controlled by nucleation reaction among Cr, S and segregated SrO on LSM electrode surface.

## 2. Experimental

Powders with following compositions were used in the work: $Y_2O_3$-$ZrO_2$ (YSZ) from Tosoh Company and $La_{0.8}Sr_{0.2}MnO_3$ from Fuel Cell Materials Company. The detailed process of fabricating half-cells can be found in our published papers [12]. Firstly, YSZ pellets were fired at 1450 °C for 5 hours with thickness of 0.5 to 0.9 mm and the diameter of 20 mm. Secondly, LSM powders were mixed with organic inks (SOFC ink vehicle, terpineol based ink vehicle, Fuel Cell Materials Company) according to the weight ratio of 50:50 to form slurries, and they were brushed onto the YSZ surface with 0.5 $cm^2$, and half-cells were fired at 1100 °C for 2 hours.

Three-electrode methods were used to test the electrocatalytic performance of the cell. Pt inks were used as counter electrodes and reference electrodes. Fe-Cr alloy (RA446) purchased was machined into coupons with channels (1.2 × 1.2 mm) and it was placed on top of the LSM electrode. Air was put into channels through an alumina tube. The cell was sealed on cathode side to prevent the leakage of $SO_2$. Dry $SO_2$ containing air (100 mL/min) (1 ppm $SO_2$) was put into the cathode. Fe-Cr alloy was regarded as the current collector when LSM electrodes were tested in the presence of Fe-Cr alloy only, Fe-Cr alloy and 1 ppm $SO_2$, while

Pt mesh was used as the current collector when LSM electrode was tested in the presence of 1 ppm $SO_2$.

At 800 ºC, the cell was tested by Gamry Reference 3000 Potentiostat to obtain the polarization and impedance curve. Impedance data were obtained from 0.1 Hz to 100 000 Hz under open circuit voltage condition. Ohmic resistances ($R_\Omega$) and electrode polarization resistances ($R_E$) were obtained with different frequencies. For comparison, the cell was tested under four conditions including ambient air, Fe-Cr alloy only, 1 ppm $SO_2$ only and Fe-Cr alloy and 1 ppm $SO_2$.

The phase of LSM electrodes before as well as after poisoning was detected by XRD from Bruker D8 Advances. XPS was tested by the ESCALAB 250Xi instrument (Thermo Fisher). SEM as well as mapping from NEON 40EsB was used to identify microstructural change of interface of LSM/YSZ and surface of YSZ electrolytes.

## 3. Results and Discussion

### *3.1 Electrocatalytic performance of LSM electrodes*

Figure 1 illustrated the electrocatalytic performance of LSM electrodes at a cathodic current of 200 mA $cm^{-2}$ in the ambient air at 800 ºC for 22 hours. According to Fig. 1a, it can be seen that overpotential decreased from 0.45 V to 0.3 V after polarizing for 2 hours, and finally changed to 0.1 V after polarization for 20 hours. The obvious reduction in the overpotential was identified by impedance behavior as well (Fig.1b and Fig.1c). $R_E$ was 18 $\Omega \cdot cm^2$ and decreased after cathodic polarization. After polarized at 200 mA $cm^{-2}$ of 2 hours, $R_E$ decreased to 5.38 $\Omega \cdot cm^2$ and achieved to 1.63 $\Omega \cdot cm^2$ for 22 hours. Moreover, $R_\Omega$ was 2.6 $\Omega \cdot cm^2$ after polarized at 200 mA $cm^{-2}$ of 22 hours.

Figure 2 showed the electrocatalytic performance for LSM cathodes in the presence of Fe-Cr alloy at cathodic current of 200 mA $cm^{-2}$ at 800 °C of 22 hours. Overpotential obviously increased from 0.3 V to 0.6 V after polarization for 2 hours, and then finally changed to 1.35 V after polarization for 22 hours. Significant increase of overpotential can be directly correlated with Cr poisoning effect of LSM electrodes, which was similar with previous results [7]. $R_E$ was 12 $\Omega \cdot cm^2$ and reduced to 6.71 $\Omega \cdot cm^2$ at 200 mA $cm^{-2}$ for 2 hours and reached to 4.52 $\Omega \cdot cm^2$ after polarization for 22 hours. Moreover, $R_\Omega$ increased from 2.41 $\Omega \cdot cm^2$ to 3.09 $\Omega \cdot cm^2$ during polarization period.

Figure 3 showed the electrocatalytic performance for LSM cathodes in the presence of 1 ppm $SO_2$ at cathodic current of 200 mA $cm^{-2}$ at 800 °C of 22 hours. Overpotential obviously increased from 0.2 V to 0.35 V under polarization for 20 h. Significant increase of overpotential can be related to S poisoning effect of LSM electrodes, which was similar with previous published results [15]. $R_E$ was 30 $\Omega \cdot cm^2$ and reduced to 3.33 $\Omega \cdot cm^2$ under polarization under 200 mA $cm^{-2}$ for 2 hours and reached to 3.38 $\Omega \cdot cm^2$ after polarization for 22 hours. Moreover, $R_\Omega$ was 2.1 $\Omega \cdot cm^2$ and kept stable during the whole polarization period. For comparison, Table 1 clearly illustrates the overpotential, $R_E$ and $R_\Omega$ in the Fe-Cr alloy and 1 ppm $SO_2$, 1 ppm $SO_2$ and Fe-Cr alloy at cathodic current of 200 mA $cm^{-2}$ at 800 °C of 22 hours. $SO_2$ deposition and poisoning on the electrochemical activity of LSM electrodes is characterized by a distinct two-stage degradation behavior (Fig.3), like that reported for $O_2$ reduction reaction on LSM electrodes in the presence of Fe-Cr metallic interconnect (Fig.2) and our previous reported literatures. $O_2$ reduction reaction on LSM electrodes was primarily controlled by oxygen dissociative adsorption and diffusion on the LSM surface. Thus,

adsorbed $SO_2$ on the active sites of LSM electrode, $SO_2$-$S_{LSM}$ would be most effective to inhibit the dissociation and diffusion of oxygen and this was indicated by the rapid increase of overpotential in Region I. The much slower increase in overpotential in Region II was most likely due to the saturation of adsorbed $SO_2$ on the electrode surface. However, the adsorbed $SO_2$, $SO_2$-$S_{LSM}$ can also be desorbed and this was indicated by the almost reproducible initial polarization behavior of overpotential as a function of cathodic current passage.

Figure 4 showed electrocatalytic performance for cathodes in the presence of Fe-Cr alloy and 1 ppm $SO_2$ at cathodic current of 200 mA $cm^{-2}$ at 800 $^oC$ for 22 hours. Overpotential obviously increased from 0.5 V to 1.5 V after being polarized for 2 h, and then changed to 1.85 V after being polarized for 22 hours. Significant increase of overpotential can be directly correlated with Cr and S poisoning effect of LSM electrodes, which was in accordance with previous published results. $R_E$ was 18 $\Omega \cdot cm^2$ and decreased to 4.56 $\Omega$ $cm^2$ at 200 mA $cm^{-2}$ for 2 hours and reached to 7.62 $\Omega \cdot cm^2$ after polarization for 22 hours. Moreover, $R_\Omega$ increased from 2 $\Omega \cdot cm^2$ to 5.1 $\Omega \cdot cm^2$ during polarization period. It is worth mentioning that the reproducible initial polarization behavior of overpotential as a function of cathodic current passage after being in the presence of Fe-Cr alloy and 1 ppm $SO_2$ was not more obvious than that of Fe-Cr alloy only and 1 ppm $SO_2$ only. As was shown before, both the adsorption and desorption rates of $SO_2$ was dependent on the temperature, one of the possible reasons that the adsorption and desorption rates was also dependent on the kinds of impurities and the different competitive adsorption/desorption of Cr and S. It can also be indicated from Fig.4 that the overpotential increased more obviously than that of Fig.2 and Fig.3, which can show

that the more severe Cr and S poisoning effect of LSM electrodes.

*3.2 Microstructural Change of LSM electrodes*

Figure 5 showed cross sectional SEM images for LSM cathodes at cathodic current of 200 mA $cm^{-2}$ in the absence of Fe-Cr alloy and 1 ppm $SO_2$ (a), the presence of Fe-Cr alloy (b), Fe-Cr alloy and 1 ppm $SO_2$ (c), 1 ppm $SO_2$ (d) at 800 ºC for 22 hours. For as-prepared LSM electrodes, the particle size of LSM was around 0.3-1 μm and particles were smooth (Fig.5a). However, there was obvious microstructural change after exposed to Fe-Cr alloy, Fe-Cr alloy and 1 ppm $SO_2$, 1 ppm $SO_2$ at 800 ºC. From Fig.5b, the LSM particles became quite rough and irregularly particles were distributed around the interface contact area. Moreover, it can be seen from Fig.5c, irregular tiny particles with size of 10-20 nm and large spinel particles with the size of 100-200 nm were clearly observed for LSM electrodes after being poisoned in combined Fe-Cr alloy and 1 ppm $SO_2$. While LSM electrodes were poisoned by $SO_2$, it can be seen that a large number of tiny particles were formed near the interface (Fig.5d). EDS results detected Cr and Zr on the interface of LSM electrodes (Fig.6b). The presence of Zr might illustrate Sr/La zirconate formation around the interface. $LaZrO_3$ was also identified around the interface of fresh LSM electrodes. Moreover, Cr and S peaks were both identified near the interface between LSM and YSZ from Fig.6c, it might indicate the forming of Sr/La sulfate or Sr/La chromite compound among the interface. According to the current result, no S peaks were clearly observed for LSM electrodes after being poisoned by $SO_2$ (Fig.6d).

*3.3 EDS and Mapping of LSM electrodes*

Figure 7 showed cross sectional SEM and EDS line scan results of LSM cathodes at cathodic current of 200 mA $cm^{-2}$ in combined Fe-Cr alloy and 1 ppm $SO_2$. According to Fig.

7b, the relative intensity of Cr and S peak (Cr,S/La) became much stronger for region 1 than region 2 and region 3, which might indicate that the Cr and S poisoning of LSM electrodes was most severe near the interface, especially near YSZ electrolytes. This result was in accordance with previous results regarding to Cr poisoning of LSM electrode under the same situation [6].

Figure 8 showed the mapping profiles of cross section for LSM cathodes at cathodic current of 200 mA $cm^{-2}$ in combined Fe-Cr alloy and 1 ppm $SO_2$ at 800 ºC for 22 hours. Cr element was easily accumulated near the interface region (LSM/YSZ), however, S element was not distributed well around the bulk of LSM electrode due to the detection limit. It can also indicate that Cr poisoning was more severe than S poisoning of LSM electrodes. This result was also in accordance with previous results regarding to Cr poisoning of LSM electrode under the same situation.

*3.4 XRD and XPS analysis of LSM electrodes*

Figure 9 shows XRD patterns for LSM electrodes at cathodic current of 200 mA $cm^{-2}$ in the absence of Fe-Cr alloy and 1 ppm $SO_2$ (a), the presence of Fe-Cr alloy (b), Fe-Cr alloy and 1 ppm $SO_2$ (c), 1 ppm $SO_2$ at 800 ºC for 22 hours. For as-prepared LSM electrodes, no other peaks were detected except LSM and YSZ peaks. For LSM electrodes after being poisoned in combined Fe-Cr alloy and 1 ppm $SO_2$, small peak around 25.6$^o$ was probably associated with $SrCrO_4$ phase, and the whole spectrum shifted a little bit comparing with curve a, which is probably related to the sample testing position difference (curves c). Moreover, regarding to the LSM electrodes after being poisoned in 1 ppm $SO_2$, $SrSO_4$ peaks appeared at both 25.5$^o$ and 44$^o$ were detected. Regarding to the LSM electrodes after being

poisoned in Fe-Cr alloy, no other peaks were identified except LSM and YSZ phase, which is due to the detection limit of XRD.

Figure 10 showed XPS spectrum of La 3d, Sr 3d, Mn 2p, Cr 2p as well as S 2p for outer and inner LSM electrodes under cathodic polarization of 200 mA $cm^{-2}$ in combined Fe-Cr alloy and 1 ppm $SO_2$ at 800 $^oC$ for 22 hours. Binding energies of La 3d agreed well with reported values for $La_{0.8}Sr_{0.2}CrO_3$ compound [27, 28]. The position for La 3d peaks were the same for outer and inner LSM electrodes at 200 mA $cm^{-2}$ in combined Fe-Cr alloy and 1 ppm $SO_2$. Mn 2p spectrums were hard to analyze by a simple deconvolution analysis regarding to $Mn^{2+}$, $Mn^{3+}$, as well as $Mn^{4+}$ compounds [28], Mn ions oxidation state could not be confirmed in this case.

For the outer surface of LSM electrodes in combined Fe-Cr alloy and 1 ppm $SO_2$, the $Sr3d_{5/2}$ peak for LSM at 132.3 eV was related to $Sr^{2+}$ ions in the lattice of LSM [29], $Sr3d_{5/2}$ peak was obtained at 134.1eV, and was related to $SrCrO_4$ or $SrSO_4$ [30], which was consistent with XRD result. While for the inner surface of LSM electrodes, the main $Sr3d_{5/2}$ peak for LSM electrodes appeared at 132.3 eV and 134.1 eV were also corresponded to $Sr^{2+}$ ions and $SrCrO_4$ or $SrSO_4$. After deconvolution of the outer surface of LSM electrodes, the binding energies of $Cr2p_{1/2}$ was 586.2 eV and 588.4 eV, while the binding energies of $Cr2p_{3/2}$ were 576.5 eV and 579.4 eV, respectively. For the binding energy of 576.5 eV for Cr $2p_{3/2}$ peak, which was consistent with $Cr^{3+}$ compounds[31]. For the binding energy of 579.4 eV for Cr $2p_{3/2}$ peak, which was correlated to $Cr^{6+}$ compounds, $Cr^{6+}$ compounds were identified by Cr $2p_{3/2}$ peaks ranging from 578.3 to 580.1 eV according to chemistry form i.e., $CrO_3$, $CrO_4^{2-}$ or $CrO_7^{2-}$. While for inner surface of LSM electrodes, binding energies of Cr $2p_{1/2}$ were 585.6

eV and 587.3 eV, respectively, while the binding energies of Cr $2p_{3/2}$ was 576.2 eV and 579.3 eV, respectively. The dominant spectra associated with $Cr^{3+}$ might indicate that Cr deposit particles were covered by $Cr_2O_3$ while the $Cr^{6+}$ was $SrCrO_4$ (Fig.9c).

Binding energy of deconvoluted S $2p_{3/2}$ peak was 168.5 eV, which was similar to the binding energy of S $2p_{3/2}$ of 168.5 eV for $SO_4^{2-}$ and the XPS results of $SrSO_4$, which was not identified by XRD results mentioned above (Fig.8c) [30]. $SrSO_4$ was observed after exposed of $La_{0.6}Sr_{0.4}CoO_{3-\delta}$ to >1ppm $SO_2$ of 24 hours [32].

*3.5 Computational Thermodynamics*

CALPHAD method has been produced on the basis of Gibbs energy minimization of single phases according to standardized Gibbs energy of pure elements in unary systems. Higher order systems can be assessed by calculated unary and binary systems. The thermodynamic databases utilized in the work have been optimized by Thermo-Calc® based on the compound energy formalism (CEF) model [33]. Two main thermodynamic databases, which are the La/Sr/Cr/Mn/O [34] and La/Sr/Mn/O [35] were examined in this work and merged with SSUB-5 database by SGTE [36]. The accuracy of all databases has been assessed by many experimental results.

*3.5.1. La-Sr-Cr-Mn-O-S Thermodynamic Database*

Assessment of La-Sr-Cr-Mn-O and La-Sr-Mn-O thermodynamic databases has been comprehensively discussed in previous works by Darvish et al. [37-39]. Similar works on La/Sr/Mn/O/C, La/Sr/Cr/Mn/O/H/S, La/Sr/Co/Fe/O/S and La/Sr/Co/Fe/O/C databases [37, 38, 40, 41] were carried out to examine the effect of atmosphere impurities, such as $CO_2$, $H_2O$ as well as chromium and $SO_2$, on LSCF and LSM perovskites. In current work, the

concept of the chromium and sulfur poisoning impact has been investigated by two thermodynamic databases listed in Table 2, i.e. (i) La/Sr/Cr/Mn/O database and (ii) La/Sr/Mn/O, which were merged with database [36]. Gibbs energies of solid phases as well as gas phase from SSUB-5 were added to (i) La/Sr/Cr/Mn/O database and (ii) La/Sr/Mn/O databases and merged La/Sr/Cr/Mn/O/S databases were assessed. The main difference of these two databases is that in database (i), the solubility of Cr in perovskite structure has been considered, therefore, the perovskite can be expressed as $(La_{1-x}Sr_x)(Mn_yCr_{1-y})O_{3\pm\delta}$; However, in database (ii) it is assumed that Cr does not dissolve into the perovskite structure and it can only react at the surface of LSM perovskite.

Accordingly, for database (i), the global equilibrium has been simulated to achieve in the system that Cr has enough time to react and dissolve in LSM perovskite and database (ii) can be applied to simulate the local equilibrium at the surface of LSM, where SrO, $MnO_x$ may precipitate out from LSM and react with Cr. In this case, the dominant reaction is controlled by the interfacial thermodynamics. Overall, predictions from both cases are critical and lead to investigate the dominant mechanism for experimental or operation conditions.

*3.5.2. Computational Thermodynamics Predictions*

In current thermodynamic prediction, phase stability of perovskite and possible secondary phases has been examined for 1 mole per formula of $La_{0.8}Sr_{0.2}MnO_{3\pm\delta}$ (LSM-20) exposed to $P_{SO_2} = 1$ ppm and 0.1 mole Cr. Figure 11-(a), corresponding to the database (i), shows that in temperature below 800 °C, $SrSO_4$ and $(Mn,Cr)_2O_3$ are highly possible to form as secondary phases in global equilibrium condition. The existence of $SrSO_4$ is directly observed from XRD analysis, while $(Mn,Cr)_2O_3$ may correlate to the $Cr^{3+}$ peak observed by

XPS results. In addition, in higher temperatures (>1050 °C) a tiny amount of spinel phase $Mn(Mn,Cr)_2O_4$ is predicted to precipitate from the perovskite. XPS results also verified the formation of $SrCrO_4$ phase for the samples tested at 800 °C, which is not observed from the prediction with database (i). It is suspected that its formation is due to the local equilibrium at the interface.

Figure 11-(b) summarizes the prediction of phase stability from the database (ii), i.e. the local equilibrium condition. It confirms formation of $SrSO_4$, $(Mn,Cr)_2O_3$ (below 800 °C), and more specifically $SrCrO_4$ as the main secondary phases in 1 ppm $SO_2$. Moreover, formation of new perovskite ($LaCrO_{3\pm\delta}$) has also been predicted above 900 °C.

Thus, from the computational thermodynamics point of view the main secondary phases, i.e. $SrSO_4$ and $Cr_2O_3$, form when LSM is exposed to 1ppm $SO_2$ and 0.1 mol Cr. However, as concentration of $SO_2$ decreases and Cr amount increases, the stability of $SrCrO_4$ rises in temperatures below 800 °C due to the local equilibrium.

*3.6 Mechanism of chromium and sulfur deposition and poisoning for LSM electrodes*

The experiment and thermodynamic calculation results of chromium and sulfur deposition and poisoning for electrodes were summarized below.

1. For LSM electrodes after polarized for 200 mA $cm^{-2}$ under different poisoning conditions including Fe-Cr alloy, Fe-Cr alloy and 1 ppm $SO_2$, 1 ppm $SO_2$, the electrocatalytic performance behaved differently. After polarized in combined Fe-Cr alloy and 1 ppm $SO_2$, overpotential obviously increased from 0.5 V to 1.85 V, $R_E$ reached to 7.62 Ω $cm^2$, and $R_\Omega$ increased from 2 Ω $cm^2$ to 5.1 Ω $cm^2$. This indicated the prominent chromium and sulfur poisoning effect on the electro catalytic

performance of LSM electrodes. $R_E$ and $R_\Omega$ both increased with polarization time for LSM electrodes in Fe-Cr alloy and 1 ppm $SO_2$.

2. XRD, XPS, EDS results indicated formation of $SrCrO_4$ and $SrSO_4$ in inner surface and outer surface for LSM electrodes under polarization at 200 mA $cm^{-2}$. Under conditions of this study, it might indicate preferential deposition of chromium and sulfur at interface of LSM/YSZ.
3. Thermodynamic computational simulation confirmed that the reaction between LSM electrodes and Fe-Cr alloy together with 1 ppm $SO_2$ is favorable, leading to the formation of $SrCrO_4$, $SrSO_4$, $(Mn,Cr)_2O_3$ at the experiment conditions. The co-existence of two mechanisms, i.e. the reactions between the perovskite and the gas impurities from local equilibrium at the interface and the global equilibrium which considered the probability of the Cr diffusion into the perovskite were predicted to govern the Cr and S poisoning of LSM.

## 4. Conclusions

In this paper, combined chromium and sulfur deposition and poisoning on the electrocatalytic performance and microstructures of LSM cathodes were investigated under cathodic polarized conditions. Chromium and sulfur species affected electrocatalytic performance and microstructures of LSM electrodes, accelerating LSM degradation, compared with chromium only and sulfur only. Chromium and sulfur depositions were likely to occur among the interface, forming $SrSO_4$/$SrCrO_4$ compounds, and caused obvious microstructural change among interface. In addition, thermodynamic computational analysis utilizing CALPHAD approach has been carried out to investigate the impact of chromium

and sulfur poisoning of LSM cathodes, which were in good agreement with experimental results.

## Acknowledgement

The authors acknowledge the supports from Curtin University and the 2018 Youth Innovation Project from Shenzhen Polytechnic (No.601822K42012), and the 2019 Youth Innovative Talents Project by Education Department of Guangdong Province, Department of Energy under Award number DE-FE0031652, and Australian Research Council (DP180100731).

## Reference

[1] Tu HY, Stimming U. Advances, aging mechanisms and lifetime in solid-oxide fuel cells. Journal of Power Sources. 2004;127:284-93.

[2] Fergus JW. Effect of cathode and electrolyte transport properties on chromium poisoning in solid oxide fuel cells. International Journal of Hydrogen Energy. 2007;32:3664-71.

[3] Schuler JA, Gehrig C, Wuillemin Z, Schuler AJ, Wochele J, Ludwig C, et al. Air side contamination in Solid Oxide Fuel Cell stack testing. Journal of Power Sources. 2011;196:7225-31.

[4] Horita T, Kishimoto H, Yamaji K, Brito ME, Xiong YP, Yokokawa H, et al. Effects of impurities on the degradation and long-term stability for solid oxide fuel cells. Journal of Power Sources. 2009;193:194-8.

[5] Brett DJL, Atkinson A, Brandon NP, Skinner SJ. Intermediate temperature solid oxide fuel cells. Chemical Society Reviews. 2008;37:1568-78.

[6] Jiang SP. Use of gaseous Cr species to diagnose surface and bulk process for $O_2$ reduction in solid oxide fuel cells. Journal of Applied Electrochemistry. 2001;31:181-92.

[7] Jiang SP, Love JG. Origin of the initial polarization behavior of Sr-doped $LaMnO_3$ for $O_2$ reduction in solid oxide fuel cells. Solid State Ionics. 2001;138:183-90.

[8] Jiang SP, Zhang JP, Zheng XG. A comparative investigation of chromium deposition at air electrodes of solid oxide fuel cells. Journal of the European Ceramic Society. 2002;22:361-73.

[9] Jiang SP, Zhang S, Zhen YD. Deposition of Cr species at $(La,Sr)(Co,Fe)O_3$ cathodes of solid oxide fuel cells. Journal of the Electrochemical Society. 2006;153:A127-A34.

[10] Liu R-R, Taniguchi S, Shiratori Y, Ito K, Sasaki K. Influence of $SO_2$ on the Long-Term Durability of SOFC Cathodes. ECS Transactions. 2011;35:2255-60.

[11] Wang FF, Yamaji K, Cho DH, Shimonosono T, Kishimoto H, Brito ME, et al. Sulfur Poisoning on $La_{0.6}Sr_{0.4}Co_{0.2}Fe_{0.8}O_3$ Cathode for SOFCs. Journal of the Electrochemical Society. 2011;158:B1391-B7.

[12] Chen KF, Ai N, Zhao L, Jiang SP. Effect of Volatile Boron Species on the Electrocatalytic Activity of Cathodes of Solid Oxide Fuel Cells I. $(La,Sr)MnO_3$ Based Electrodes. Journal of the Electrochemical Society. 2013;160:F183-F90.

[13] Chen KF, Ai N, Zhao L, Jiang SP. Effect of Volatile Boron Species on the Electrocatalytic Activity of Cathodes

of Solid Oxide Fuel Cells II. (La,Sr)(Co,Fe)$O_3$ Based Electrodes. Journal of the Electrochemical Society. 2013;160:F301-F8.
[14] Wang CC, Chen KF, Jiang SP. Sulfur Deposition and Poisoning of $La_{0.6}Sr_{0.4}Co_{0.2}Fe_{0.8}O_{3-\delta}$ Cathode Materials of Solid Oxide Fuel Cells. Journal of the Electrochemical Society. 2014;161:F1133-F9.
[15] Wang CC, Chen K, Jiang SP. Mechanism and Kinetics of $SO_2$ Poisoning on the Electrochemical Activity of $La_{0.8}Sr_{0.2}MnO_3$ Cathodes of Solid Oxide Fuel Cells. Journal of the Electrochemical Society. 2016;163:F771-F80.
[16] Xiong YP, Yamaji K, Horita T, Yokokawa H, Akikusa J, Eto H, et al. Sulfur Poisoning of SOFC Cathodes. Journal of the Electrochemical Society. 2009;156:B588-B92.
[17] Bucher E, Gspan C, Hofer F, Sitte W. Sulphur poisoning of the SOFC cathode material $La_{0.6}Sr_{0.4}CoO_{3-\delta}$. Solid State Ionics. 2013;238:15-23.
[18] Wang F, Yamaji K, Cho DH, Shimonosono T, Nishi M, Kishimoto H, et al. Evaluation of Sulfur Dioxide Poisoning for LSCF Cathodes. Fuel Cells. 2013;13:520-5.
[19] Kishimoto H, Wang F, Cho D-H, Lv P, Bagarinao KD-, Yamaji K, et al. Degradation of LSCF Cathode Induced by $SO_2$ in Air. ECS Transactions. 2015;68:1045-50.
[20] Mori N, Sato Y, Iha M, Takada T, Konoike T, Kishimoto H, et al. Sulfur Poisoning of LSCF Cathode in Single Step Co-fired SOFC. ECS Transactions. 2015;68:1015-22.
[21] Yokokawa H. Achievements of NEDO Projects on SOFC Durability. Meeting Abstracts. 2017;MA2017-03:338.
[22] Chen XB, Zhang L, Liu EJ, Jiang SP. A fundamental study of chromium deposition and poisoning at $(La_{0.8}Sr_{0.2})_{(0.95)}(Mn_{1-x}Co_x)O_{3\ (+/-\delta)}$ (0.11 <= x 1.0) cathodes of solid oxide fuel cells. International Journal of Hydrogen Energy. 2011;36:805-21.
[23] Jiang SP, Chen XB. Chromium deposition and poisoning of cathodes of solid oxide fuel cells - A review. International Journal of Hydrogen Energy. 2014;39:505-31.
[24] Wei B, Chen KF, Wang CC, Lu Z, Jiang SP. Cr deposition on porous $La_{0.6}Sr_{0.4}Co_{0.2}Fe_{0.8}O_{3-\delta}$ electrodes of solid oxide cells under open circuit condition. Solid State Ionics. 2015;281:29-37.
[25] Daio T, Mitra P, Lyth SM, Sasaki K. Atomic-resolution analysis of degradation phenomena in SOFCS: A case study of $SO_2$ poisoning in LSM cathodes. International Journal of Hydrogen Energy. 2016;41:12214-21.
[26] Wang CC, O'Donnell K, Jian L, Jiang SP. Co-Deposition and Poisoning of Chromium and Sulfur Contaminants on $La_{0.6}Sr_{0.4}Co_{0.2}Fe_{0.8}O_{3-\delta}$ Cathodes of Solid Oxide Fuel Cells. Journal of the Electrochemical Society. 2015;162:F507-F12.
[27] Gunasekaran N, Bakshi N, Alcock CB, Carberry JJ. Surface characterization and catalytic properties of perovskite type solid oxide solutions, $La_{0.8}Sr_{0.2}BO_3$ (B = Cr, Mn, Fe, Co or Y). Solid State Ionics. 1996;83:145-50.
[28] Murray JW, Dillard JG, Giovanoli R, Moers H, Stumm W. Oxidation of Mn(II): Initial mineralogy, oxidation state and ageing. Geochimica Et Cosmochimica Acta. 1985;49:463-70.
[29] Wu Q-H, Liu M, Jaegermann W. X-ray photoelectron spectroscopy of $La_{0.5}Sr_{0.5}MnO_3$. Materials Letters. 2005;59:1980-3.
[30] Wang CC, O'Donnell K, Jian L, Jiang SP. Co-Deposition and Poisoning of Chromium and Sulfur Contaminants on $La_{0.6}Sr_{0.4}Co_{0.2}Fe_{0.8}O_{3-\delta}$ Cathodes of Solid Oxide Fuel Cells. Journal of The Electrochemical Society. 2015;162:F507-F12.
[31] Chapin DS, Kafalas JA, Honig JM. Electrical Properties of Ferromagnetic $CrO_x$ (1.89 < x < 2.02). The Journal of Physical Chemistry. 1965;69:1402-9.
[32] Bucher E, Gspan C, Hofer F, Sitte W. Sulphur poisoning of the SOFC cathode material $La_{0.6}Sr_{0.4}CoO_{3-\delta}$. Solid State Ionics. 2013;238:15-23.
[33] Hillert M. The Compound Energy Formalism. Journal of Alloys and Compounds. 2001;320:161-76.

[34] Karadeniz EP. Thermodynamic Database of the La-Sr-Mn-Cr-O Oxide System and Applications to Solid Oxide Fuel Cells: Swiss Federal Institute of Technology Zurich; 2008.
[35] Grundy AN. CALPHAD Assessment of the La - Sr - Mn - O System and the Defect Chemistry of (La, Sr)$MnO_3$ Perovskites used as Solid Oxide Fuel Cell Cathode Materials. Zurich: Swiss Institute of Technology; 2003.
[36] Europe SGT. SGTE Substances Database-SSUB5. Thermo-Calc.
[37] Darvish S, Hu B, Singh P, Zhong Y. Thermodynamic and Experimental Evaluation of $La_{1-x}Sr_xMnO_{3\pm\delta}$ Cathode in the Presence of Cr-Containing Humidified Air. Journal of Minerals, Metals & Materials Society. 2018:1-11.
[38] Darvish S, Asadikiya M, Hu B, Singh P, Zhong Y. Thermodynamic prediction of the effect of $CO_2$ to the stability of (La0.8Sr0.2)0.98MnO3±δ system. International Journal of Hydrogen Energy. 2016;41:10239-48.
[39] Darvish S, Sabarou H, Saxena SK, Zhong Y. Quantitative Defect Chemistry Analysis and Electronic Conductivity Prediction of $La_{0.8}Sr_{0.2}MnO_{3\pm\delta}$ Perovskite. Journal of The Electrochemical Society. 2015;162:E134-E40.
[40] Darvish S, Asadikiya M, Yang M, Zhong Y. The Application of Computational Thermodynamics to the Cathode-Electrolyte in Solid Oxide Fuel Cells. Nanostructured Materials for Next-Generation Energy Storage and Conversion: Springer; 2018. p. 281-335.
[41] Lu Z, Darvish S, Hardy J, Templeton J, Stevenson J, Zhong Y. $SrZrO_3$ Formation at the Interlayer/Electrolyte Interface during $(La_{1-x}Sr_x)_{1-\delta}Co_{1-y}Fe_yO_3$ Cathode Sintering. Journal of The Electrochemical Society. 2017;164:F3097-F103.

**Figures and Table captions**

**Table 1.** The summarized ohmic resistance and electrode polarization resistance for LSM electrodes in the presence of Fe-Cr alloy, 1 ppm $SO_2$, Fe-Cr alloy and 1 ppm $SO_2$ at a cathodic current of 200 mA $cm^{-2}$ for 22 hours at 800 $^oC$ (electrode was also polarized in the ambient air as comparison).

**Table 2.** Databases Description.

**Figure 1.** Polarization as well as impedance curves for $O_2$ reduction reaction on porous LSM cathodes at a cathodic current of 200 mA $cm^{-2}$ for 22 hours at 800 $^oC$ in the ambient air.

**Figure 2.** Polarization and impedance curves for $O_2$ reduction reaction of porous LSM cathodes in Fe-Cr alloy at a cathodic current of 200 mA $cm^{-2}$ for 22 hours at 800 $^oC$.

**Figure 3.** Polarization and impedance curves of porous LSM cathodes in the presence of 1 ppm $SO_2$ at a cathodic current of 200 mA $cm^{-2}$ for 22 hours at 800 $^oC$.

**Figure 4.** Polarization and impedance curves of porous LSM cathodes in the presence of Fe-Cr alloy and 1 ppm $SO_2$ at a cathodic current of 200 mA $cm^{-2}$ for 22 hours at 800 $^oC$.

**Figure 5.** Cross sectional SEM micrographs of LSM cathodes at a cathodic current of 200 mA $cm^{-2}$ in the ambient air (a), presence of Fe-Cr alloy (b), presence of Fe-Cr alloy and 1 ppm $SO_2$ (c), presence of 1 ppm $SO_2$ (d) at 800 $^oC$ for 22 hours.

**Figure 6.** EDS spectra of selected areas cross sectional LSM cathodes at a cathodic current of 200 mA $cm^{-2}$ in the ambient air (a), presence of Fe-Cr alloy (b), presence of Fe-Cr alloy and 1 ppm $SO_2$ (c), presence of 1 ppm $SO_2$ (d) at 800 $^oC$ for 22 hours.

**Figure 7.** (a) Cross-sectional SEM images of LSM cathodes and (b) EDS line scan profiles of selected area of (a). LSM was polarized at a cathodic current of 200 mA $cm^{-2}$ in the presence

of Fe-Cr alloy and 1 ppm $SO_2$ at 800 $^oC$ for 22 hours.

**Figure 8.** Cross-section of mapping image of LSM cathodes at a cathodic current of 200 mA $cm^{-2}$ at 800 $^oC$ in the presence of presence of Fe-Cr alloy and 1 ppm $SO_2$ at 800 $^oC$ for 22 hours.

**Figure 9.** XRD patterns of LSM cathodes at a cathodic current of 200 mA $cm^{-2}$ at 800 $^oC$ in the ambient air (a), presence of Fe-Cr alloy (b), presence of Fe-Cr alloy and 1 ppm $SO_2$ (c), presence of 1 ppm $SO_2$ (d) at 800 $^oC$ for 22 hours.

**Figure 10.** High resolution XPS spectrum of La3d, Sr3d, Mn2p, S2p as well as Cr2p for outer (a) and inner (b) surface of LSM cathodes at a cathodic current of 200 mA $cm^{-2}$ at 800 $^oC$ for 22 hours in the presence of Fe-Cr alloy and 1 ppm $SO_2$.

**Figure 11.** Phase stability diagrams for 1 mole per formula of LSM-20 at 1 ppm $SO_2$ and 0.1 mole Cr utilizing (a) database (i) (b) database (ii).

**Table 1**.

| Polarized time | 800 °C fresh | | 800 °C Cr | | 800°C Cr+S | | 800 °C S | |
|---|---|---|---|---|---|---|---|---|
| | $R_\Omega/\Omega..cm^2$ | $R_E/\Omega.cm^2$ | $R_\Omega/\Omega.cm^2$ | $R_E/\Omega.cm^2$ | $R_\Omega/\Omega.cm^2$ | $R_E/\Omega.cm^2$ | $R_\Omega/\Omega.cm^2$ | $R_E/\Omega.cm^2$ |
| **0 min** | 1.84 | 18.17 | 2.38 | 13.23 | 2.01 | 18.67 | 1.8 | 30 |
| **5 min** | 1.86 | 14 | 2.39 | 12.51 | 2.02 | 8.48 | 1.9 | 18.12 |
| **10 min** | 1.86 | 8.19 | 2.41 | 11.65 | 2.07 | 6.85 | 1.95 | 6.3 |
| **20 min** | 1.89 | 5.8 | 2.45 | 10.24 | 2.85 | 6.0 | 1.96 | 4.65 |
| **30 min** | 1.93 | 5.47 | 2.47 | 8.81 | 2.90 | 5.21 | 1.97 | 3.72 |
| **1 h** | 2.07 | 5.38 | 2.46 | 6.71 | 3.10 | 4.56 | 1.98 | 3.33 |
| **4 h** | 2.66 | 3.99 | 2.68 | 3.69 | 3.25 | 4.80 | 1.98 | 2.75 |
| **8 h** | 2.67 | 2.98 | 2.84 | 3.61 | 3.50 | 6.22 | 2 | 2.86 |
| **12 h** | 2.62 | 2.43 | 2.94 | 4.02 | 4.1 | 6.48 | 2.02 | 3.02 |
| **16 h** | 2.64 | 1.96 | 3.01 | 4.5 | 4.7 | 7.46 | 2.06 | 3.18 |
| **20 h** | 2.63 | 1.64 | 3.09 | 4.52 | 5.1 | 7.62 | 2.1 | 3.38 |

**Table 2.**

| Database Name | Main Elements | Elements Added from SSUB-5 |
|---|---|---|
| Database (i) | La-Sr-Cr-Mn-O | S |
| Database (ii) | La-Sr-Mn-O | S, Cr |

**Figure 1.**

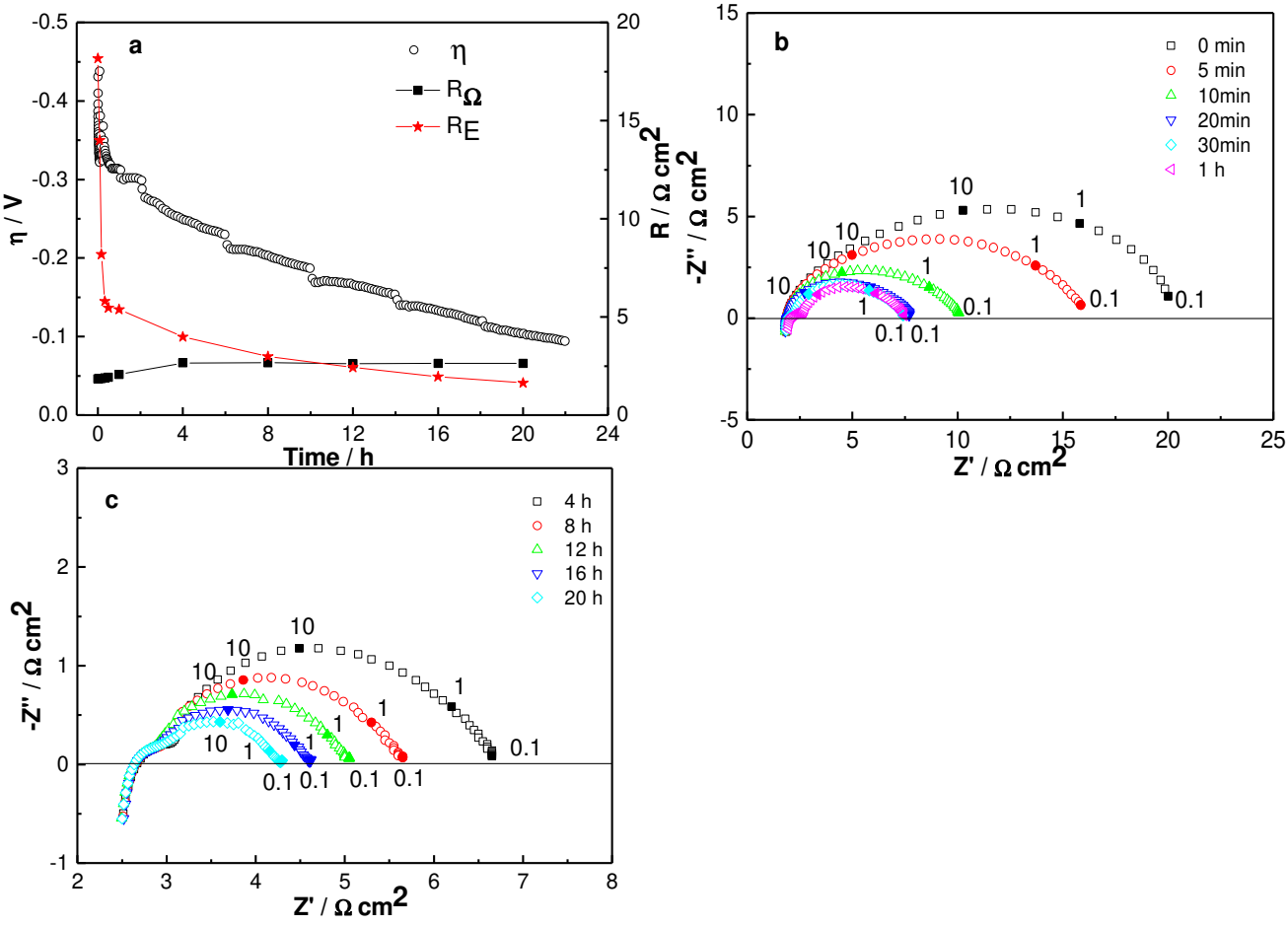
a
η
$R_\Omega$
$R_E$
η / V
R / Ω cm2
Time / h
b
0 min
5 min
10min
20min
30min
1 h
-Z'' / Ω cm2
Z' / Ω cm2
c
4 h
8 h
12 h
16 h
20 h
-Z'' / Ω cm2
Z' / Ω cm2

**Figure 2.**

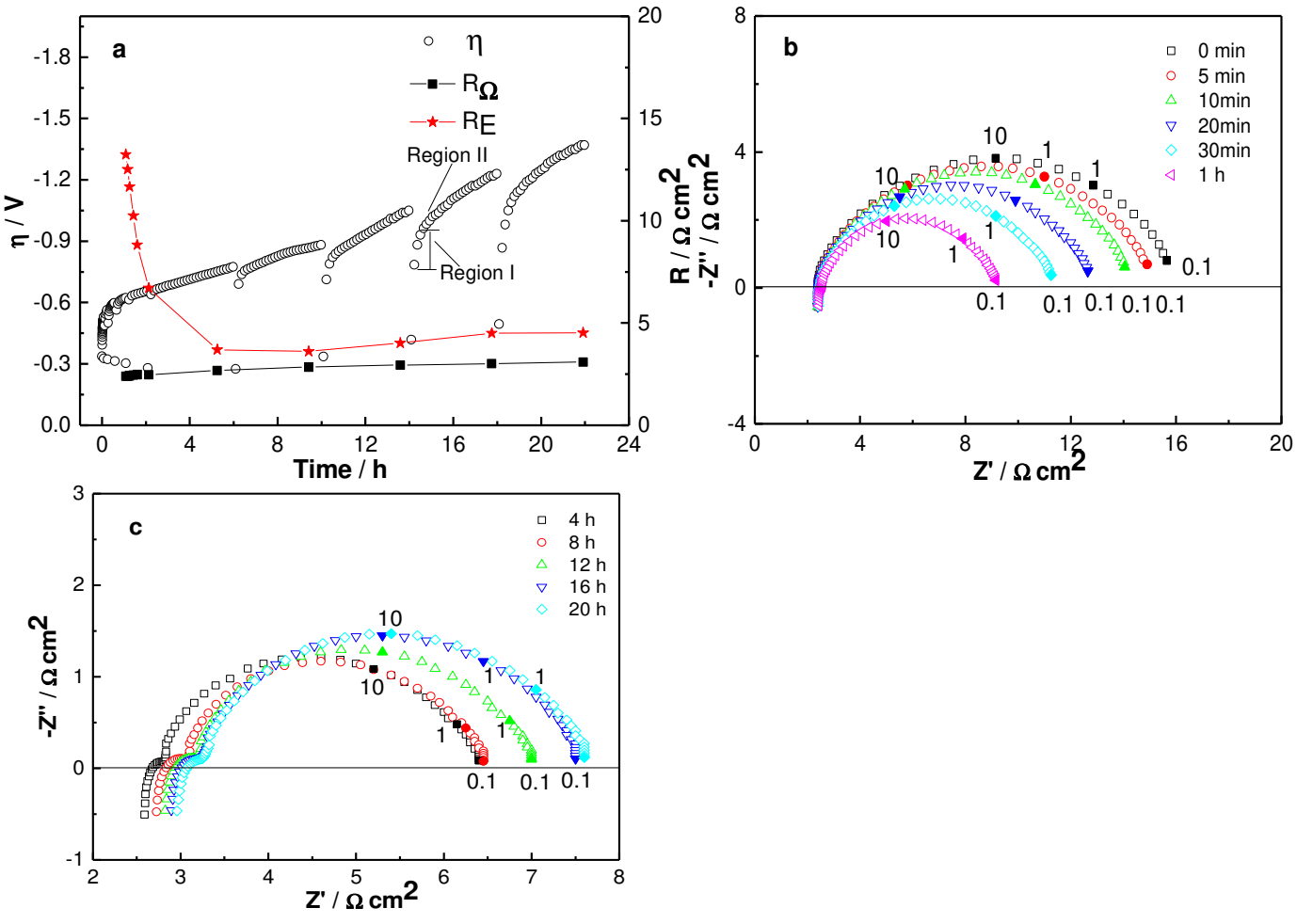
a
η
$R_\Omega$
$R_E$
Region II
Region I
η / V
Time / h
b
0 min
5 min
10min
20min
30min
1 h
R / Ω cm2
-Z'' / Ω cm2
Z' / Ω cm2
c
4 h
8 h
12 h
16 h
20 h
-Z'' / Ω cm2
Z' / Ω cm2

**Figure 3.**

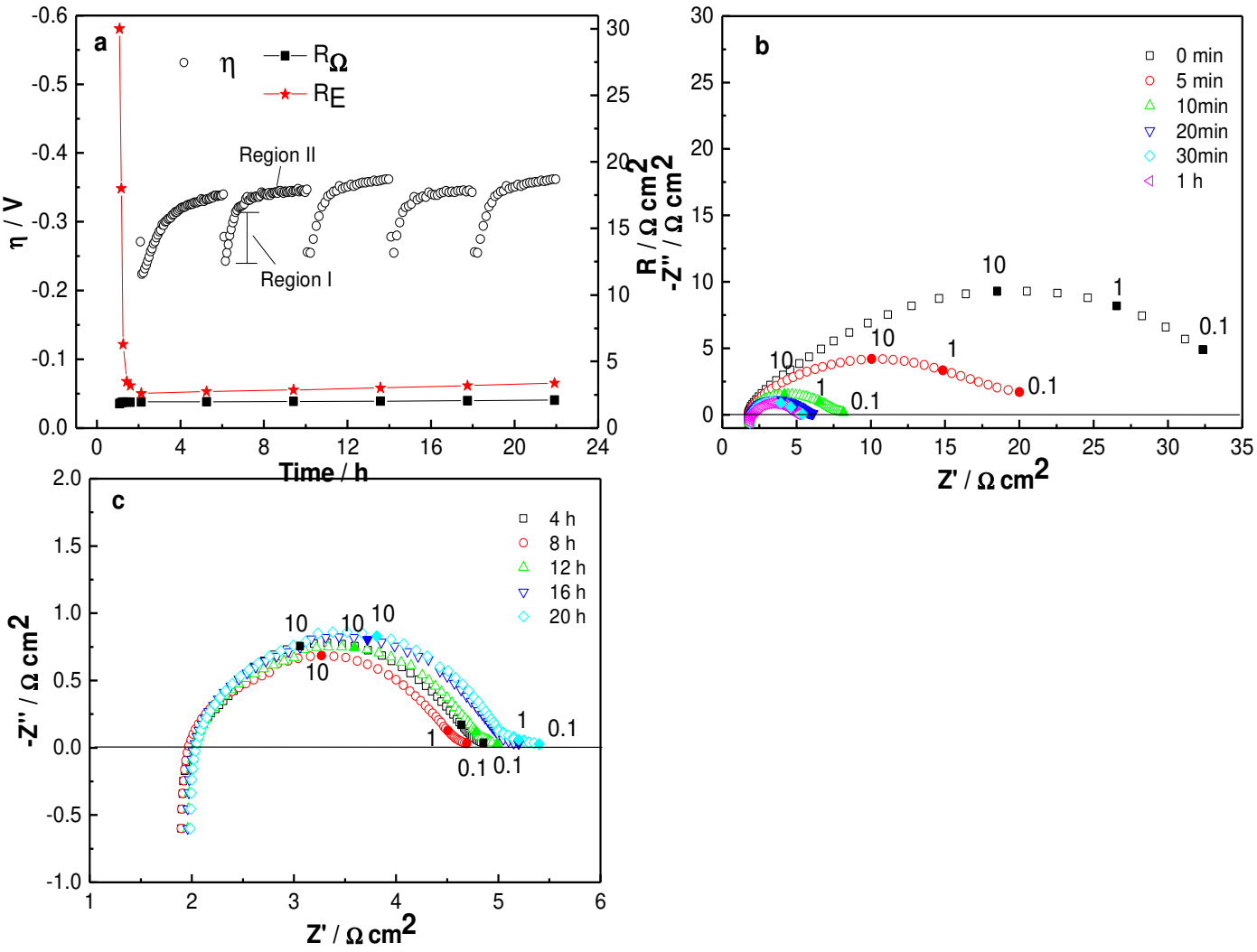
a
η
$R_\Omega$
$R_E$
Region II
Region I
η / V
R / Ω cm2
Time / h
b
0 min
5 min
10min
20min
30min
1 h
-Z'' / Ω cm2
Z' / Ω cm2
c
4 h
8 h
12 h
16 h
20 h
-Z'' / Ω cm2
Z' / Ω cm2

**Figure 4.**

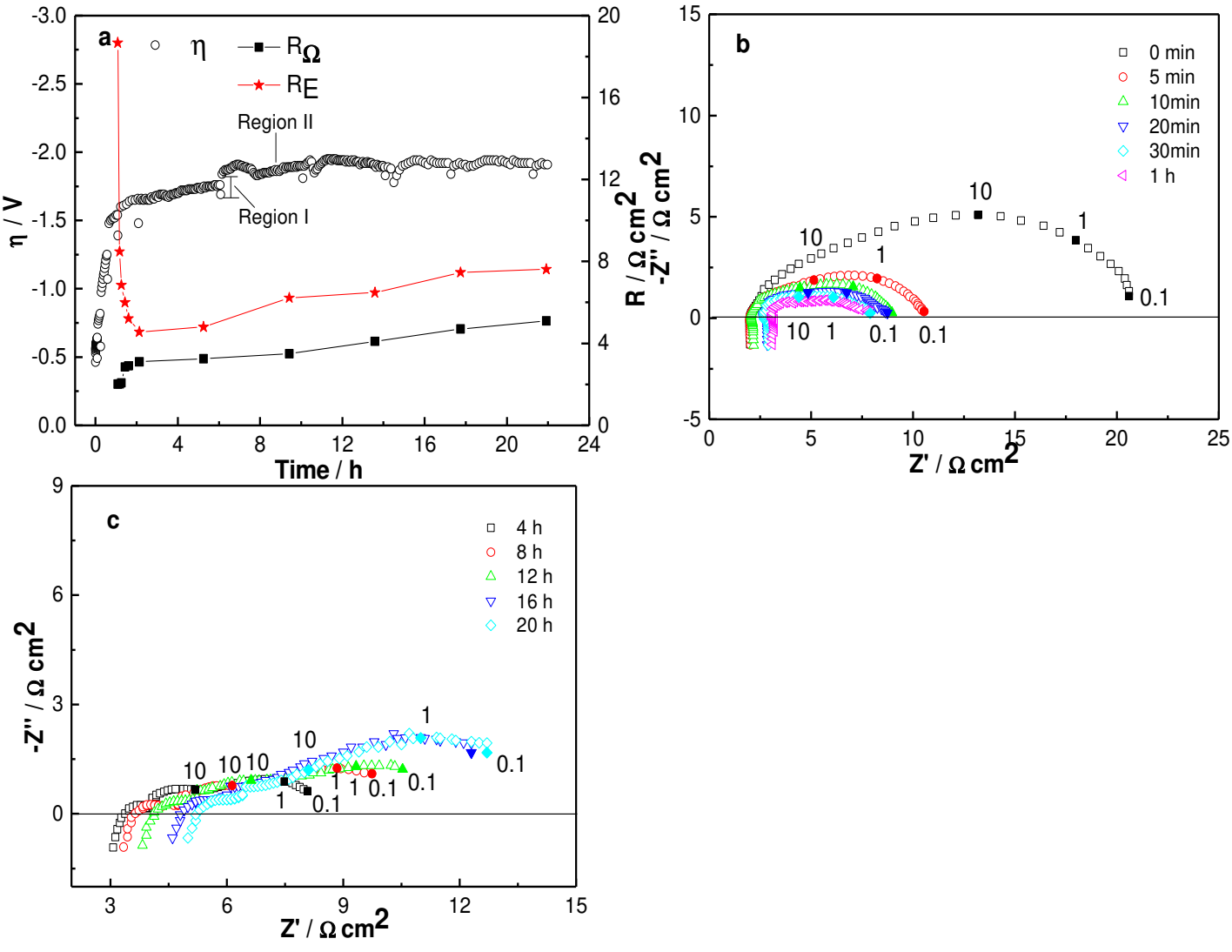
a
η
$R_\Omega$
$R_E$
Region II
Region I
η / V
R / Ω cm2
Time / h
b
0 min
5 min
10min
20min
30min
1 h
-Z'' / Ω cm2
Z' / Ω cm2
c
4 h
8 h
12 h
16 h
20 h
-Z'' / Ω cm2
Z' / Ω cm2

**Figure 5.**

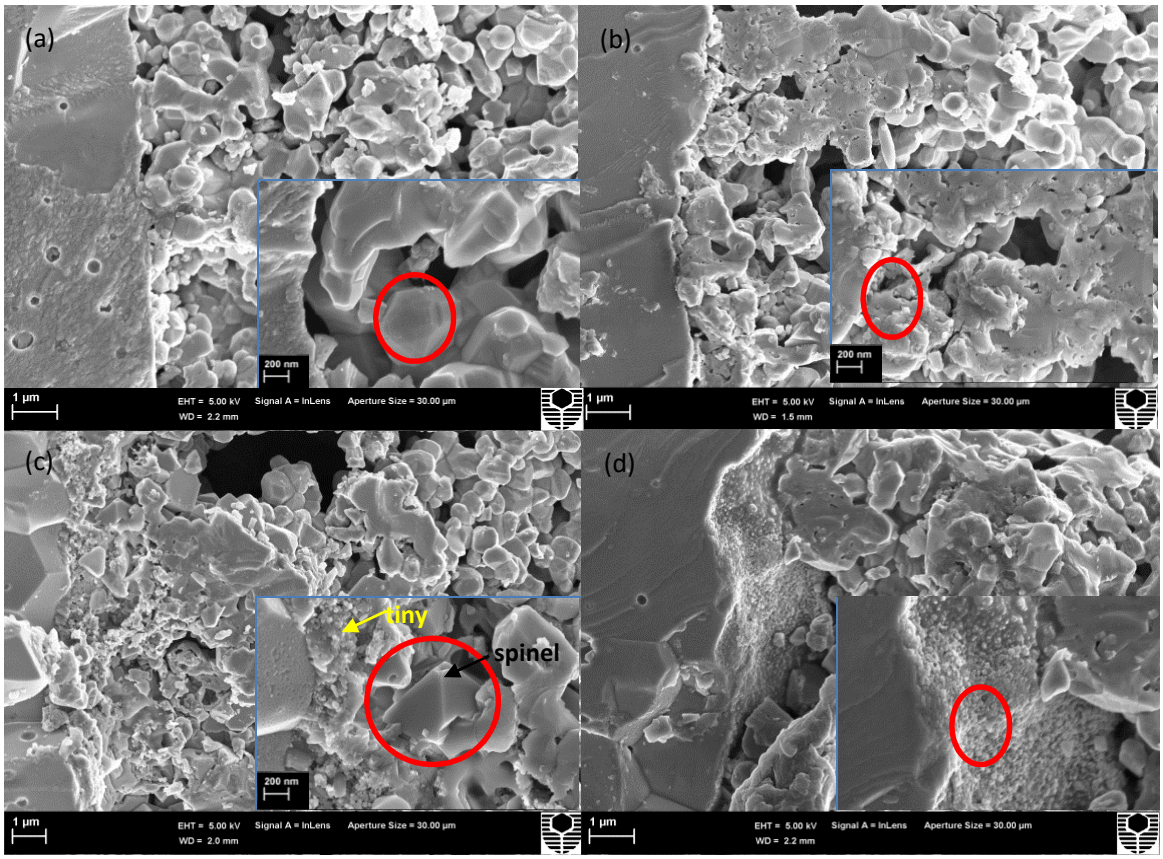
(a)
200 nm
1 µm
EHT = 5.00 kV
WD = 2.2 mm
Signal A = InLens
Aperture Size = 30.00 µm
(b)
200 nm
1 µm
EHT = 5.00 kV
WD = 1.5 mm
Signal A = InLens
Aperture Size = 30.00 µm
(c)
tiny
spinel
200 nm
1 µm
EHT = 5.00 kV
WD = 2.0 mm
Signal A = InLens
Aperture Size = 30.00 µm
(d)
1 µm
EHT = 5.00 kV
WD = 2.2 mm
Signal A = InLens
Aperture Size = 30.00 µm

**Figure 6.**

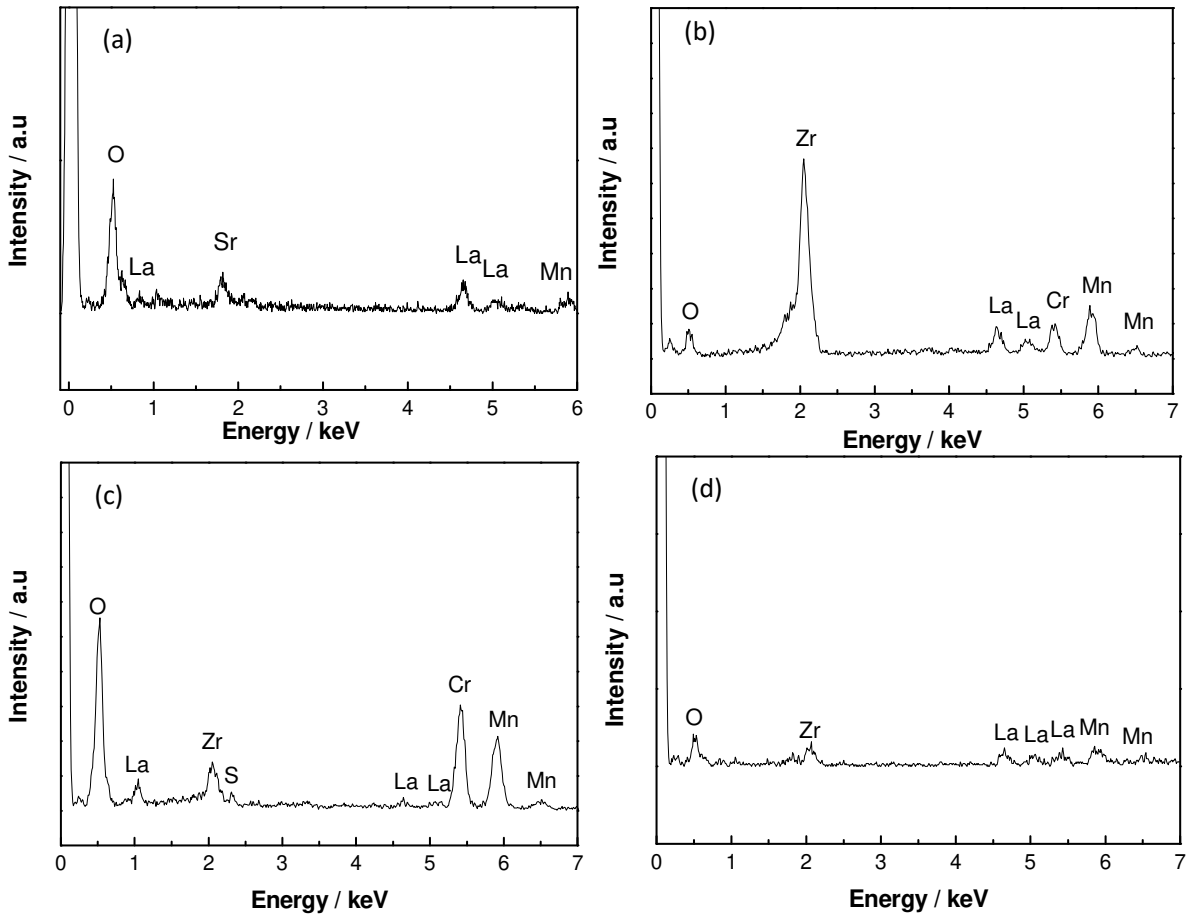
(a)
O
La
Sr
La
La
Mn
Intensity / a.u
Energy / keV
(b)
Zr
O
La
La
Cr
Mn
Mn
Intensity / a.u
Energy / keV
(c)
O
La
Zr
S
La
La
Cr
Mn
Mn
Intensity / a.u
Energy / keV
(d)
O
Zr
La
La
La
Mn
Mn
Intensity / a.u
Energy / keV

**Figure 7.**

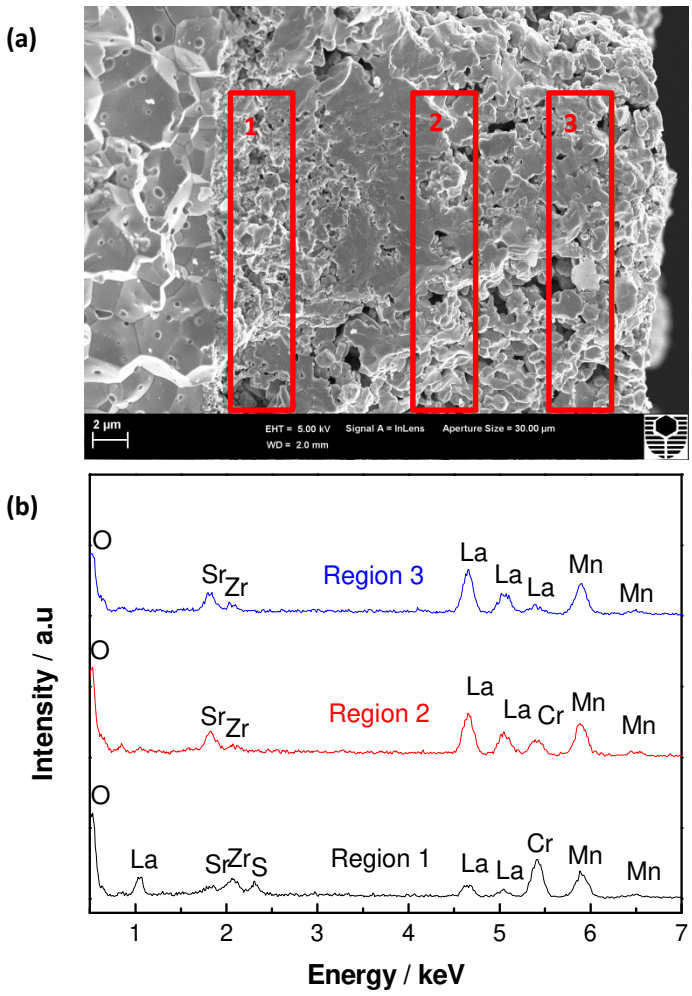
(a)
1
2
3
2 µm
EHT = 5.00 kV
WD = 2.0 mm
Signal A = InLens
Aperture Size = 30.00 µm
(b)
Intensity / a.u
O
Sr Zr
Region 3
La
La
La
Mn
Mn
O
Sr Zr
Region 2
La
La
Cr
Mn
Mn
O
La
Sr Zr S
Region 1
La
La
Cr
Mn
Mn
1
2
3
4
5
6
7
Energy / keV

**Figure 8.**

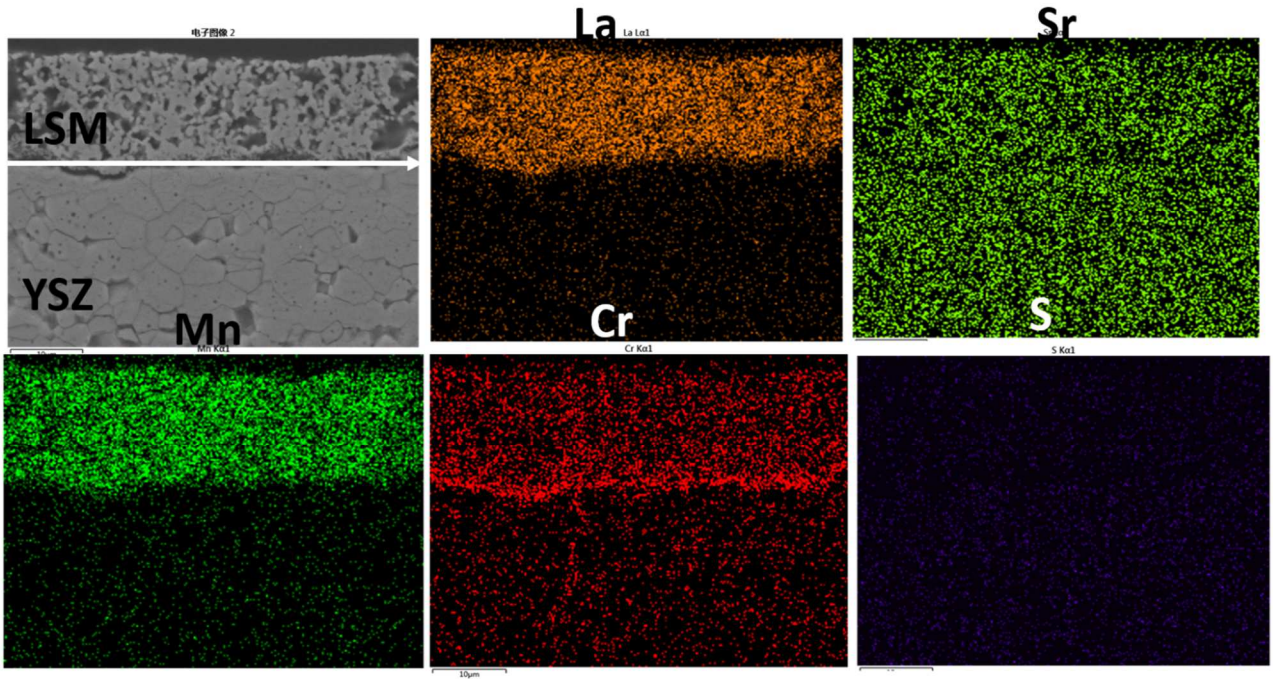

**Figure 9.**

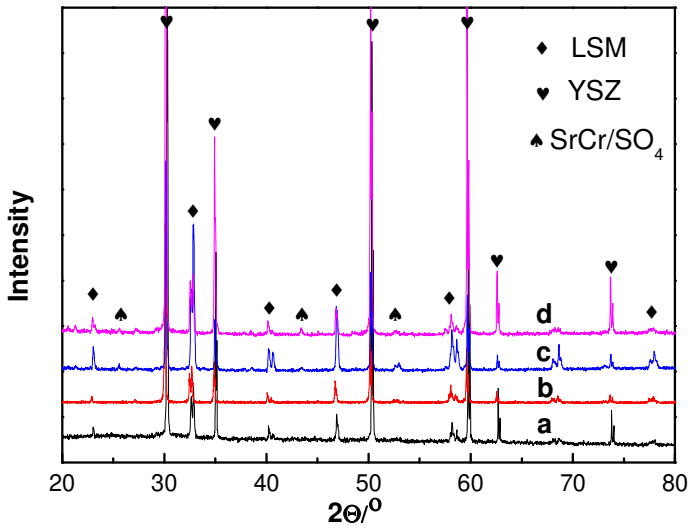

**Figure 10.**

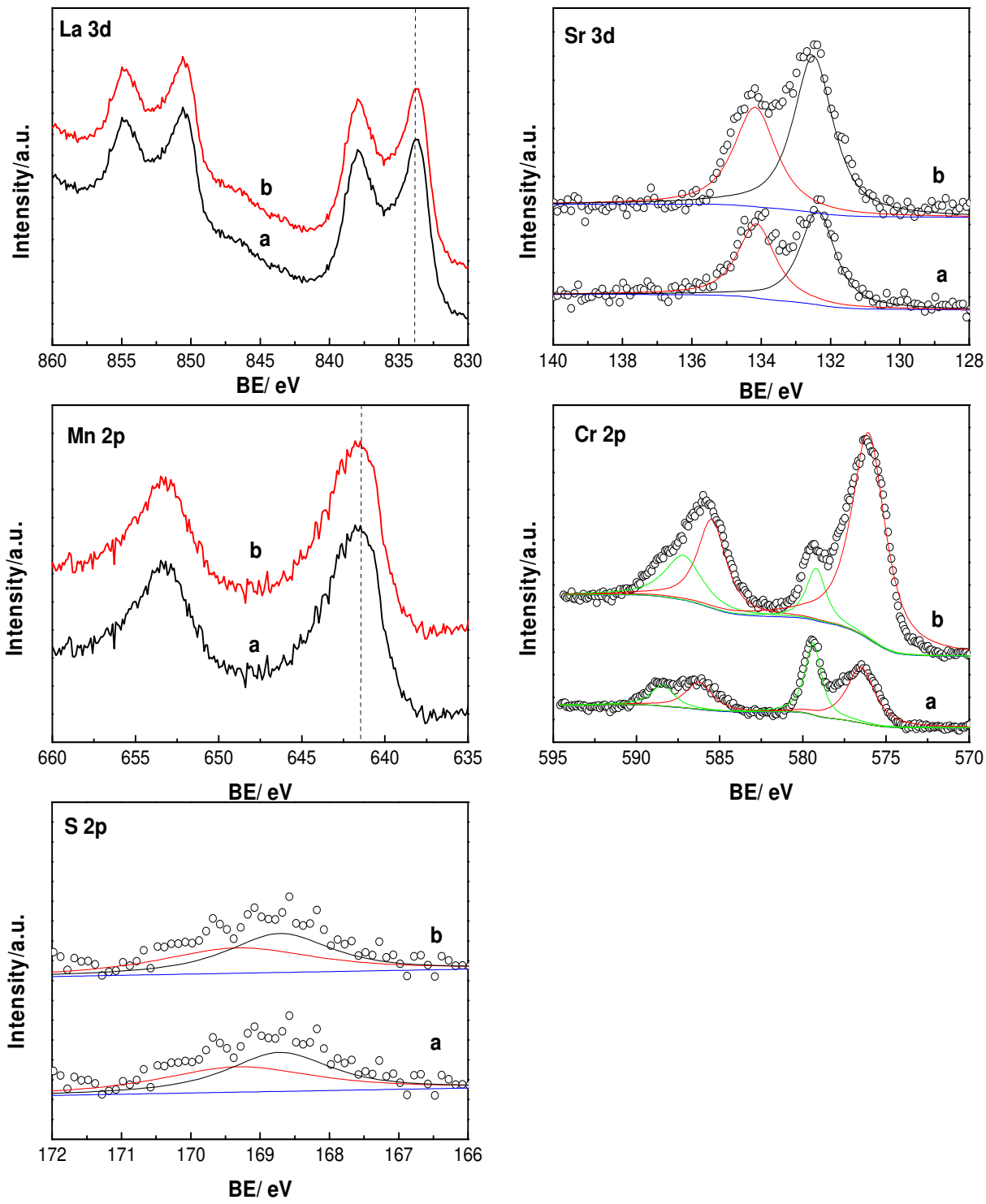
La 3d
Intensity/a.u.
b
a
860
855
850
845
840
835
830
BE/ eV
Sr 3d
Intensity/a.u.
b
a
140
138
136
134
132
130
128
BE/ eV
Mn 2p
Intensity/a.u.
b
a
660
655
650
645
640
635
BE/ eV
Cr 2p
Intensity/a.u.
b
a
595
590
585
580
575
570
BE/ eV
S 2p
Intensity/a.u.
b
a
172
171
170
169
168
167
166
BE/ eV

**Figure 11.**

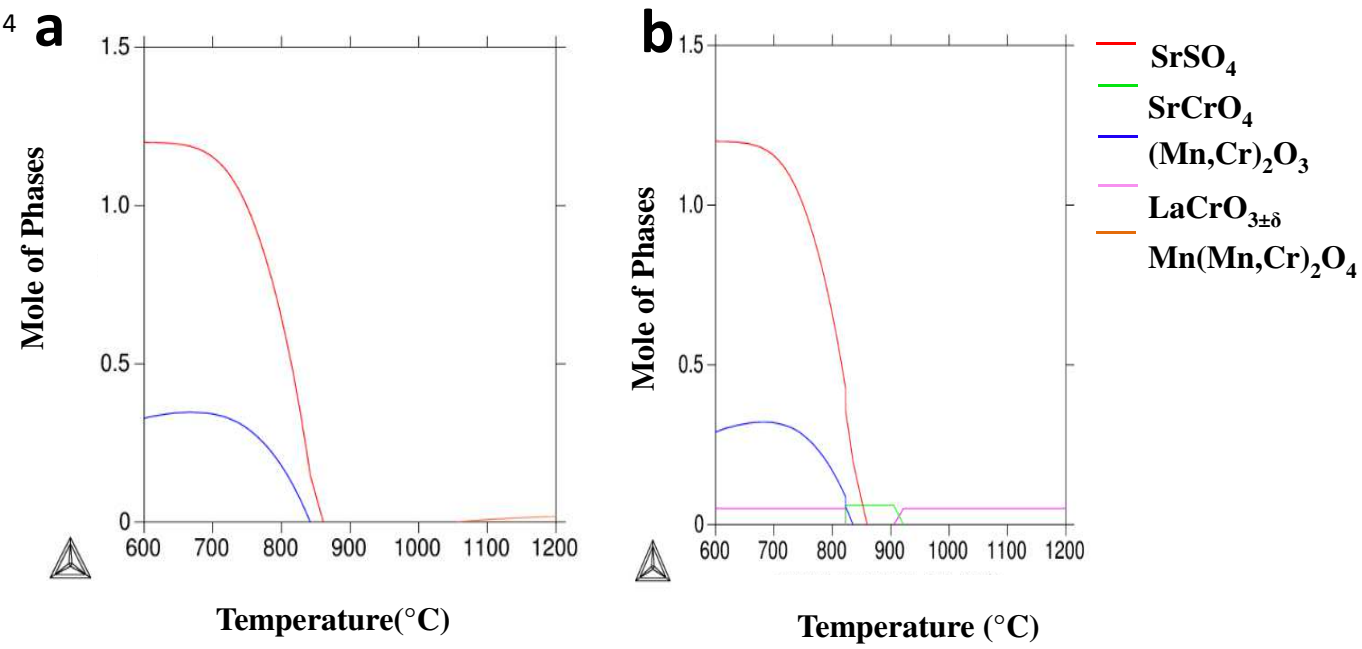
a
b
Mole of Phases
1.5
1.0
0.5
0
600
700
800
900
1000
1100
1200
Temperature(°C)
Temperature (°C)
SrSO4
SrCrO4
(Mn,Cr)2O3
LaCrO3±δ
Mn(Mn,Cr)2O4